

# ACS Nano, volume 10, pages 1033–1041, year 2016 // Synthesis of Pyrene-Fused Pyrazaacenes on Metal Surfaces: Toward One-Dimensional Conjugated Nanostructures

Li Jiang,<sup>1</sup> Anthoula C. Papageorgiou,<sup>1, a)</sup> Seung Cheol Oh,<sup>1</sup> Özge Sağlam,<sup>1</sup> Joachim Reichert,<sup>1, b)</sup> David A. Duncan,<sup>1</sup> Yi-Qi Zhang,<sup>1</sup> Florian Klappenberger,<sup>1</sup> Yuanyuan Guo,<sup>1</sup> Francesco Allegretti,<sup>1</sup> Sandeep More,<sup>2, 3</sup> Rajesh Bhosale,<sup>3</sup> Aurelio Mateo-Alonso,<sup>2, 4, c)</sup> and Johannes V. Barth<sup>1</sup>

<sup>1)</sup>Physik Department E20, Technische Universität München, 85748 Garching, Germany

<sup>2)</sup>POLYMAT, University of the Basque Country UPV/EHU, Avenida de Tolosa 72, E-20018 Donostia-San Sebastian, Spain

<sup>3)</sup>Freiburg Institute for Advanced Studies (FRIAS), School of Soft Matter Research, and Institut für Organische Chemie und Biochemie, Albert-Ludwigs-Universität Freiburg, Albertstraße 19, 79104 Freiburg, Germany

<sup>4)</sup>Ikerbasque, Basque Foundation for Science, Bilbao, Spain

We investigated the synthesis of one-dimensional nanostructures via Schiff base (imine) formation on three close-packed coinage metal (Au, Ag, and Cu) surfaces under ultrahigh vacuum conditions. We demonstrate the feasibility of forming pyrene-fused pyrazaacene-based oligomers on the Ag(111) surface by thermal annealing of tetraketone and tetraamine molecules, which were designed to afford cyclocondensation products. Direct visualization by scanning tunneling microscopy of reactants, intermediates, and products with submolecular resolution and the analysis of their statistical distribution in dependence of stoichiometry and annealing temperature together with the inspection of complementary X-ray photoelectron spectroscopy signatures provide unique insight in the reaction mechanism, its limitations, and the role of the supporting substrate. In contrast to the reaction on Ag(111), the reactants desorb from the Au(111) surface before reacting, whereas they decompose on the Cu(111) surface during the relevant thermal treatment.

Keywords: imine, Schiff base, cyclocondensation, STM, XPS, ultrahigh vacuum

Since the discovery of fullerenes in 1985,<sup>1</sup> there has been an intense effort in exploring low-dimensional conjugated carbon materials and tapping the full potential of their properties. More recently, graphene-related materials, in particular, graphene nanoribbons doped with heteroatoms,<sup>2–6</sup> have been the focus of intensive research, as the introduction of nitrogen atoms (N-doping) can be used to tailor their electronic structure,<sup>7</sup> which is an essential requirement for the development of future organic electronics based on graphene circuits. These materials also provide electrochemically active systems with properties useful for batteries and fuel cells. Furthermore the tunable and exceptionally high light absorption in the visible range makes them promising candidates as absorbing layers in organic photovoltaics.<sup>8</sup> However, the exploration of potential pathways for the targeted design of such nanostructured devices still needs intense investigations to progress from being a purely academic playground to ensuring technological impact of low-dimensional graphene-based materials.

Pyrene-fused pyrazaacenes<sup>9</sup> (PPAs) are among this type of nitrogenated ribbon-like structures (Scheme 1c).

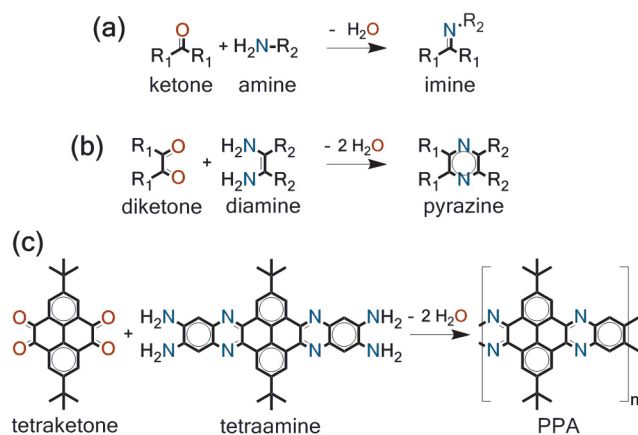


FIG. 1. \*

Scheme 1. (a) Condensation of a Ketone and an Amine, (b) Cyclocondensation Reaction of a Diketone and Diamine, and (c) Cyclocondensation Reaction of the Tetraketone and the Tetraamine Molecules Employed Here into PPAs

Besides their tunable optoelectronic properties, PPAs have shown a very high stability, which makes them an ideal platform to develop narrow one-dimensional materials. PPA-based oligomers<sup>10–16</sup> (with up to 16 linearly fused aromatic rings) and polymers<sup>17–19</sup> have been synthesized through solution-based methods by means of imine-type cyclocondensations (Scheme 1b).

Nevertheless, PPAs are very insoluble materials with a

<sup>a)</sup>Electronic mail: a.c.papageorgiou@tum.de

<sup>b)</sup>Electronic mail: joachim.reichert@tum.de

<sup>c)</sup>Electronic mail: amateo@polymat.eu

great tendency to aggregate, which hampers their synthesis and characterization. Therefore, on-surface synthetic methods provide an alternative aggregation-free environment not only for producing PPAs but also for characterizing their structure with submolecular resolution, allowing the identification and study of intermediates and defects.

On-surface organic synthesis has bloomed over the past decade.<sup>20–26</sup> Some of the most recent topical endeavors utilized azide–alkyne couplings,<sup>27,28</sup> couplings involving C–H activation of alkynes,<sup>29</sup> alkenes,<sup>30,31</sup> and alkanes,<sup>32,33</sup> enediyne cyclizations followed by polymerization,<sup>34</sup> as well as decarboxylative polymerization.<sup>35</sup> In particular, Schiff base (imine) formations (Scheme 1a) have been successfully implemented for low-dimensional structures at solid–liquid interfaces.<sup>36–43</sup> Imine formation under these conditions has a dynamic character which relies on the reversibility of the relevant covalent bonds under thermodynamic control.<sup>44</sup> Therefore, this type of bonding combines the increased stability of covalent bonds with the potential of producing regular superstructures. These characteristics place it among the most promising routes for covalent molecular architectonics, and imines have been demonstrated to form under vacuum conditions, as well.<sup>45–47</sup> Specifically, an aldehyde and octylamine on Au(111) surfaces form the imine product readily at room temperature (RT),<sup>45</sup> whereas cyclocondensation reactions (Scheme 1b) have been reported for thick films of suitable diamine and diketone molecules at temperatures above  $\sim 373$  K.<sup>46</sup>

Herein, we investigate the reaction of 2,7-di-*tert*-butylpyrene-4,5,9,10-tetraketone (tetraketone) and 2,11-di-*tert*-butylquinoxalino[2',3':9,10]phenanthro[4,5-*abc*]phenazine-6,7,15,16-tetraamine (tetraamine) for the *in situ* formation of PPAs (Scheme 1c) on coinage metal surfaces of varying reactivity, resulting in varying efficacy. We show that on the Ag(111) surface it yields PPA-based oligomers with up to 19 linearly fused rings. This illustrates the potential of this methodology not only to produce long PPA-based oligomers but also, most importantly, to characterize their structure with great detail including structural defects in order to further improve their synthesis. Our experimental study relies on detailed molecular-level imaging by temperature-controlled scanning tunneling microscopy (STM) and spectroscopic analysis by high-resolution X-ray photoelectron spectroscopy (XPS).<sup>48</sup>

## RESULTS AND DISCUSSION

### Visualization of Reactants and Reaction Products.

Initially, the STM appearance of the monomers employed was determined by dosing tetraketone and tetraamine molecules separately on the Ag(111) surface. Figure 1a shows a representative STM image zooming in

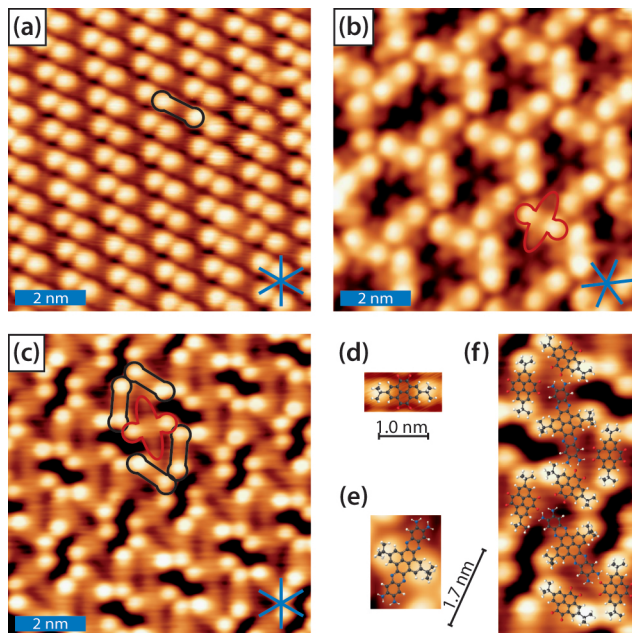


FIG. 1. STM topography of tetraketone and tetraamine molecules on Ag(111) substrate after deposition at RT. The blue lines indicate the high symmetry axes of the substrate. In (a–c), single tetraketone and single tetraamine molecules are outlined in black and red, respectively. (a) STM image of densely packed tetraketone molecules ( $T_{\text{STM}} \sim 170$  K,  $U_s = 1.25$  V,  $I_t = 0.16$  nA). (b) Self-assembly of tetraamine molecules ( $T_{\text{STM}} \sim 110$  K,  $U_s = 1.54$  V,  $I_t = 0.11$  nA). (c) Two-dimensional nanostructures of tetraketone intermixed with tetraamine ( $T_{\text{STM}} \sim 160$  K,  $U_t = 2.89$  V,  $I_t = 0.12$  nA). (d–f) Zoom in STM images (d, tetraketone; e, tetraamine; f, mixture of tetraketone and tetraamine) overlaid with corresponding ball-and-stick models.

a densely packed island of tetraketones, from which we can identify the molecules lying with their  $\pi$ -bonded moieties nearly parallel to the surface. For both molecules, the contrast is dominated by the physically protruding *tert*-butyl groups that are imaged as bright lobes, whereas the molecular backbone is resolved more faintly. Figure 1d depicts a single tetraketone molecule, superposed with the proposed molecular ball-and-stick model. The tetraamine molecule has a different  $\pi$ -conjugated system, which is imaged in the STM topographical images as a faint oval shape between the two *tert*-butyl bright protrusions (Figure 1e). In Figure 1b, one can clearly identify tetraamine molecules clustered together, with their faint oval backbones orientated along the high symmetry directions of the substrate. STM investigations of the tetraamine show molecules only within these intricate molecular arrangements, which appeared after RT deposition and were maintained up to annealing temperatures as high as 530 K. A detailed analysis of the supramolecular self-assembly scenarios of the tetraketone and the tetraamine molecules is beyond the scope of the present article and will be presented elsewhere.

In order to promote the cyclocondensation reactions,

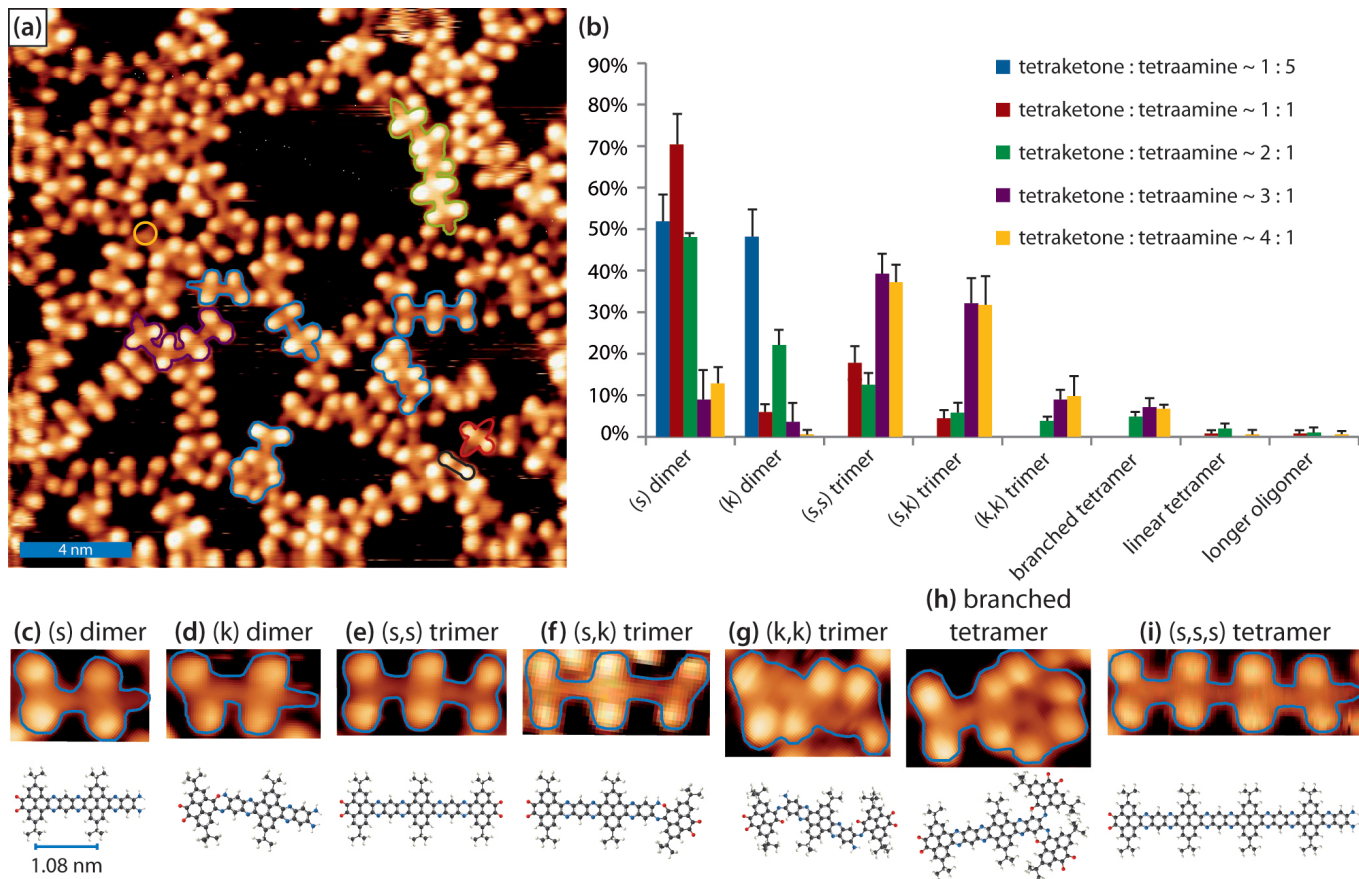


FIG. 2. Condensation products of tetraketone and tetraamine. (a) Overview of imine formation reactions on Ag(111) after annealing to 510 K with a stoichiometry of tetraketone to tetraamine  $\sim 2 : 1$  ( $T_{\text{STM}} = \text{RT}$ ,  $U_s = 2.22 \text{ V}$ ,  $I_t = 0.09 \text{ nA}$ ). (b) Histogram of different oligomers generated after annealing to 510 K as a function of the molecular ratio of tetraketone to tetraamine. (c–i) STM images and molecular models of the main types of oligomers resolved after annealing. (The calculation of the standard deviation used can be found in the Supporting Information.)

submonolayer coverages of tetraketone and tetraamine molecules were deposited onto the Ag(111) surface at RT and subsequently annealed gradually to 510 K. At room temperature, the two molecules readily intermix in regular bimolecular assemblies (Figure 1c,f), which are observed even after annealing up to 510 K. In addition, after this treatment, different kinds of oligomers furnish the surface. Figure 2a shows an overview in which we can discern some distinct oligomers, for instance, a straight (s) dimer, a bent (k) dimer, a straight (s,s) trimer, a bent (k,k) trimer, and a branched (b) tetramer, whose boundaries are outlined by blue solid lines. Here, (s) and (k) denote a straight connection between the monomers and a kink in the connection, respectively. Furthermore, one pentamer (outlined in green in Figure 2a) can be observed, in which two (s) dimers are coupled with one tetraamine. Apart from these oligomers, there are still unreacted monomers (see molecules outlined by black and red contours in Figure 2a). Some undesired side reaction appears between free terminal amines, which fused together after this annealing treatment, as highlighted by yellow circle; the amine groups from two (s) dimers and a

(k) dimer appear linked altogether. Overall, the surface is dominated by dimers and trimers (see also Figure 2b). However, trimers terminated with diamine moieties are statistically insignificant, a point to which we will return later.

The STM data and molecular models in Figures 2c–i give a simplified classification of the occurring oligomers. Due to its linear shape and the distance between its *tert*-butyl groups (marked in Figure 2c), which was measured to be approximately 1.08 nm, the dimer labeled (s) is assigned to the product of the desired cyclocondensation. In contrast, (k) dimers assume a kinked conformation, presumably because only one ketone reacted with one amine to form a single imine. This dimer has two different conformations: the one that allows the ketone moiety to have an intramolecular interaction with the neighboring amine moiety (shown in Figure 2d) and one that does not (shown in Supporting Information Figure S1). Figure 2e–g categorizes the types of trimers based on the number of cyclocondensations and single imine formations, similar to the categorization of the dimers. For example, (k,k) has two kinks, where both the tetraketone molecule

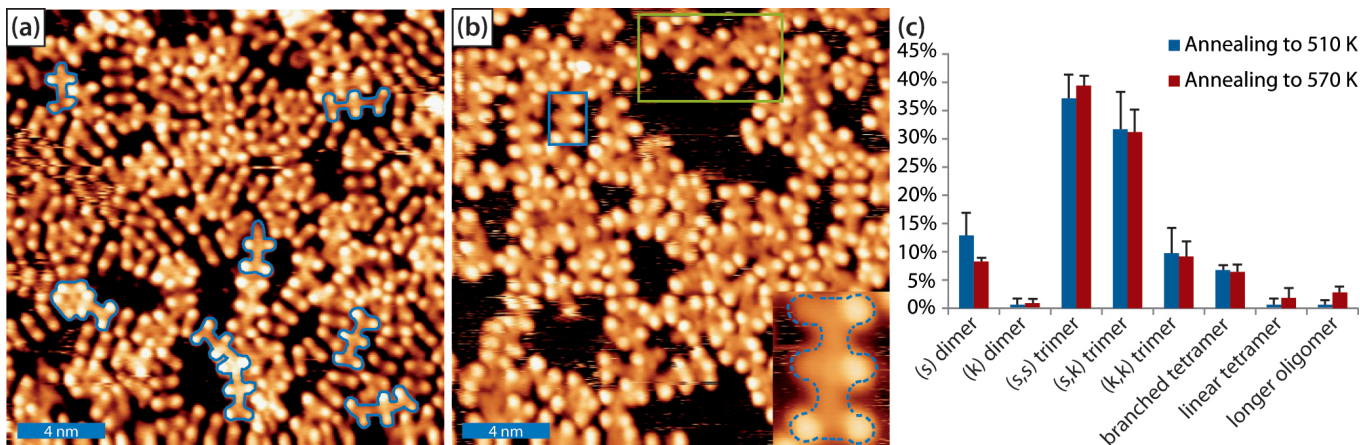


FIG. 3. Effect of annealing temperature on the polymerization process. (a) STM image showing condensation products after dosing tetraketone and tetraamine in  $\sim 4 : 1$  stoichiometry on Ag(111) and then annealing to 510 K ( $T_{\text{STM}} = \text{RT}$ ,  $U_s = 1.54$  V,  $I_t = 0.03$  nA). (b) Overview of this surface after further annealing to 570 K ( $T_{\text{STM}} = \text{RT}$ ,  $U_s = 1.24$  V,  $I_t = 0.12$  nA). The inset displays a magnified image of the blue box with a straight trimer with two partially decomposed *tert*-butyl groups outlined by a dashed blue line. (c) Distribution of different oligomer species as a function of annealing temperature. (The calculation of the standard deviation used can be found in the Supporting Information.)

moieties are tilted relatively to the central tetraamine molecule, and every tetraketone was linked by a single imine with each side of tetraamine. The tetramers are divided in two types: those that are branched (Figure 2h), where one tetraamine is surrounded by three tetraketones, and those that are linear, in which two tetraketones alternately link with two tetraamines. In addition to the illustrated (s,s,s) tetramer with 19 linearly fused rings in Figure 2i, linear tetramers containing single imines instead of pyrazine rings existed, similar to those found in the (k) dimer and in (s,k) and (k,k) trimers. For example, in Figure 2a, a (s,k,k) tetramer is outlined in purple.

To investigate the effect of stoichiometry, we tuned the tetraketone to tetraamine ratio from  $\sim 1 : 5$  to  $\sim 4 : 1$ . The distribution of different oligomer species as a function of stoichiometry is shown in Figure 2b. From that, we can infer the following: First, we note that in the same oligomer category, and for every investigated stoichiometry, the straight type is more probable than the corresponding bent type. This effect is more pronounced for dimers but can also be distinguished for the longer oligomers. It indicates that the cyclocondensation is preferred to the single imine formation, albeit with less selectivity the longer the oligomer. This selectivity could originate in the ring closure (Scheme 1b) being a sequential reaction of  $1 + 1$  imine formation reaction, in which the product with the single imine (Scheme 1a) is a stable intermediate. Importantly, these types of ketoimine intermediates obtained from *o*-phenylenediamines have not been isolated from solution-based synthetic methods. Second, we observed that increasing the proportion of tetraketone molecules increased the yield of trimers. On a surface with an excess of tetraamine molecules, 75% of the surface tetraketone molecules reacted to form dimers

(blue histogram in Figure 2b, Supporting Information Table S1), but no longer oligomers were observed. Initially, the formation of dimers seems to be the favorable product at the annealing temperature of 510 K; however, especially in the presence of excess tetraketone, we observed that the same treatment results in the addition of the tetraketone monomers to the dimer amine side. The yield of the tetraamine modules within the oligomers at  $1 : 1$ ,  $2 : 1$ ,  $3 : 1$ , and  $4 : 1$  (tetraketone/tetraamine) stoichiometry was 35, 54, 60, and 69%, respectively, whereas the percentage of amine to imine conversion is 20, 29, 47, and 54%, respectively; that is, as the relative amount of tetraketone increases, both the amount of (partially) reacted tetraamine molecules and the amount of formed imines increase. In all of the cases, there is a limited number of terminal amines in the polymers, showing that the condensation of an amine module (or oligomer) with a diketone terminated oligomer is unfavorable.

Furthermore, we investigated the influence of the annealing temperature on the polymerization process. Figure 3a reveals the condensation products after dosing tetraketone and tetraamine molecules in a  $\sim 4 : 1$  stoichiometry and then annealing to 510 K. We can distinguish the two types of dimers, the three kinds of trimers, the branched tetramer, and a bent (s,s,k,s) pentamer (highlighted by blue solid lines). Subsequent further annealing to 570 K desorbed most of the unreacted tetraketone and modestly promoted lengthening of the oligomers, as illustrated in Figure 3. This is also reflected on the percentage of tetraamine molecules incorporated into oligomers, which increased from 69 to 79% after this higher temperature annealing.

The histogram in Figure 3c presents the trend of oligomer formation with the annealing temperature. By inspection, we can deduce that part of (s) dimers re-

acted with the available tetraketone, forming trimers, especially straight (s,s) trimers. Although the differences observed in the histogram are within the statistical error, the trend deduced is consistent. This heat treatment also affected a significant portion of the *tert*-butyl groups. This is illustrated by the straight trimer outlined in blue in the inset of Figure 3b, where two *tert*-butyl groups are resolved faintly in comparison with the intact ones. In some areas (example shown in the green box in Figure 3b), the molecular decomposition prevents us from identifying the oligomer shape. With increased annealing temperature, more tetraketone molecules desorbed from the surface, limiting the elongation of the polymers. (See also Table S1 in Supporting Information for an account of all surface species.) We therefore corroborate our earlier conclusion that longer oligomers require a second stage, higher temperature annealing. In this situation, no excess tetraketone is left on the surface, but it is still possible to condense dimers and trimers into forming longer oligomers ( $n = 5$ ) and/or to condense tetraamine monomers to existing oligomers.

The annealing temperatures required for the cyclocondensation reaction on Ag (510 K) are significantly higher than the ones reported for similar cyclocondensation reactions on thick molecular films under vacuum (373 K),<sup>46</sup> as well as in solution ( $\sim 323 - 453$  K).<sup>10-14,16</sup> Accordingly, we dosed molecules in three layers (tetraketone-tetraamine-tetraketone), which turns out to produce a very limited number of dimers at lower temperatures (400 K). After this annealing treatment, only molecules in direct contact with the metal surface remained. As no condensation products were observed after annealing a submonolayer of tetraketone and tetraamine molecules to 400 K, we can conclude that the condensation reaction requires much lower thermal energy in the case that the two reacting modules are not confined in the two-dimensional geometry imposed when they are adsorbed on the metal surface. Indeed, on the Ag(111) surface, the reaction seems to proceed at the temperature of the onset of desorption of the tetraketone molecule. It is estimated by STM images that annealing to 510 K causes a 10-20% loss of the surface tetraketone molecules. No decrease in coverage was observed for the tetraamine molecules under the same conditions, thus implying that they are more strongly bound to the Ag(111) surface. Assuming that the reaction needs a nonplanar intermediate, as expected for the classical imine formation between a ketone and an amine (Supporting Information Figure S2), this would require a lift-off of the  $\pi$ -conjugated backbone from the surface. (We note that, on Ag(111) and Cu(111), the surface itself can abstract protons from the molecular moieties.<sup>49,50</sup>) In fact, this assumption would justify why diamine-terminated oligomers longer than dimers rarely form and why the polymerization is limited: the tetraketone  $\pi$ -conjugated backbone is the easiest to lift-off from the surface, whereas more extended modules adsorb more strongly on the surface. More than 98% of all s or k joints observed after annealing at 510 K can be accounted for

with the addition of a tetraketone monomer to a longer module.

To explore the effect of the underlying metal surface, we also investigated this reaction on gold and copper. A monolayer of tetraketone and tetraamine molecules with a ratio of 6 : 1 was dosed on the Au(111) substrate, but no oligomers formed because the tetraketone molecule desorbed rather than reacted with tetraamine after stepwise heating up to 610 K (Supporting Information Figure S3). After being annealed to 610 K, the surface contained almost exclusively tetraamine molecules with numerous *tert*-butyl groups decomposed. On the Cu(111) surface, both molecules were deposited in 1 : 1 stoichiometry. However, no oligomers formed after annealing up to 490 K, although a number of *tert*-butyl groups decomposed under this annealing treatment (Supporting Information Figure S4). Based on these results, we infer that Ag binds the monomers strongly enough for them to react on the surface, but not so strong as to inhibit the lift-off necessary for the imine formation. In contrast, on Au the tetraketone monomer desorbed during higher temperature annealing. On Cu, the monomers have a higher affinity to the metal surface and therefore already decompose at annealing temperatures below the condensation temperature found on Ag(111). Additionally, the lift-off of the ketone might be hindered on Cu due to the stronger coupling.

### Probing the Chemical State of Reactants.

Complementary XPS characterization of these reactants on Ag(111) and Au(111) sheds light on the reaction mechanism.

Figure 4 shows the N 1s XP spectra of the tetraamine adsorbed on Ag(111) at RT and after annealing treatment (420 K). The N 1s spectrum of the tetraamine after RT deposition shows two components of similar intensity, one centered at a binding energy of  $400.1 \pm 0.1$  eV due to the primary aminic N ( $-C - NH_2$ )<sup>51</sup> and the other centered at a binding energy of  $398.9 \pm 0.1$  eV attributed to iminic N ( $-C = N - C =$ ).<sup>52,53</sup> Conversely, after being annealed to 420 K, the deconvolution of the spectrum shows three components (Figure 4b). In addition to the aminic and the iminic N, a weaker peak appears at  $397.8 \pm 0.1$  eV, associated with the presence of  $-N^-H$ .<sup>53,54</sup> It thus appears that the Ag surface activates the amines by partial deprotonation, acting as a "base" by removing the positive charge, which is expected to promote the desired imine formation. In such a case, the condensation reaction would proceed slightly differently on the Ag surface than in solution (Supporting Information Figure S2), with  $H_2$  as one of the byproducts at lower temperature.<sup>29</sup>

Furthermore, the adsorption of the tetraketone molecules was studied by XPS on Ag(111) and Au(111); the corresponding C 1s and O 1s XP spectra are shown in Figure 5. On Au(111), the C 1s spectrum shows three contributions at binding energies of 284.1, 284.6,

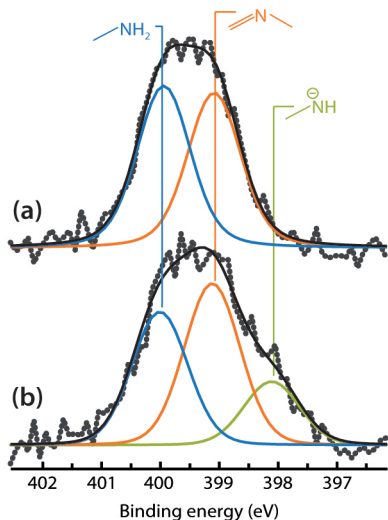


FIG. 4. XP spectra of the N 1s core level of a submonolayer coverage of tetraamine on Ag(111) after RT deposition (a) and after annealing to 420 K (b). A photon energy of 550 eV was used for the acquisition.

and 286.9 eV, which can be attributed to the presence of aromatic,<sup>30,55</sup> aliphatic,<sup>55,56</sup> and carbonylic carbon atoms,<sup>57,58</sup> respectively, with a ratio of approximately 3 : 2 : 1. The O 1s spectrum instead displays a single peak centered at a binding energy of 531.2 eV corresponding to carbonylic O ( $-\text{C}=\text{O}$ ).<sup>58,59</sup> On Ag(111), this peak shifts to lower binding energy by  $\sim 1$  eV, which is ascribed to hybridization of the  $\text{C}=\text{O}$  group with the substrate metal states ( $\text{C}=\text{O}^-\cdots\text{M}^+$ ).<sup>58</sup> Additionally, a shoulder can be noticed at  $\sim 531.5$  eV: the intensity of this feature was found to grow with increasing beam exposure, therefore, we attribute it to radiation damage. Regrettably, the occurrence of radiation damage precludes a further conclusive XPS investigation of the changes observed after annealing to temperatures that promote the imine formation.

The hybridized state is presumably associated with the formation of an extended  $\pi$ -conjugated system that is strongly coupled to the underlying metal. The C 1s spectrum also indicates that the peak related to carbon atoms bonded to oxygen shifted to lower binding energy by  $\sim 1.8$  eV, further confirming that the bond of these carbon atoms to oxygen is significantly weaker than that in carbonyl moieties. From the comparison, we infer that the hybridized oxygen is beneficial to this polymerization reaction, probably because the tetraketone molecules can remain in the vicinity of the Ag(111) surface upon annealing to higher temperatures, and thereafter, they can adopt the optimal geometric configuration relative to tetraamines to activate the imine formation reaction before desorbing from the surface. In contrast, there is no hybridized oxygen on Au(111), and as a consequence of the weaker anchoring, the tetraketone molecules desorb from the surface before reacting with tetraamines.

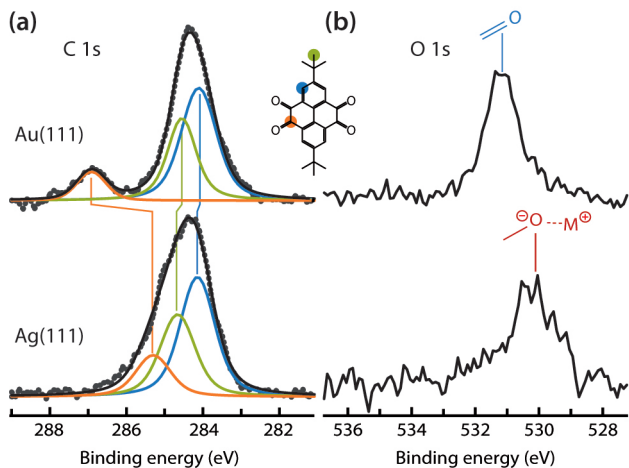


FIG. 5. XP spectra of the C 1s (a) and O 1s (b) core levels, corresponding to a submonolayer coverage of tetraketone on Au(111) (top) and Ag(111) (bottom) after RT deposition. In the C 1s signal, three different contributions can be resolved in the fitting. The corresponding peaks are colored as the highlights of the respective C atoms in the molecular model. All spectra were acquired using monochromatized Al  $K\alpha$  radiation.

## SUMMARY AND CONCLUSIONS

In conclusion, this work has demonstrated the feasibility of preparing PPA-based oligomers on the Ag(111) surface under ultrahigh vacuum (UHV) conditions. From STM images, we inferred that the metal surface imposes a planar adsorption geometry of both the tetraketone and the tetraamine monomers, which hinders the imine formation. From XPS measurements, we concluded that the Ag(111) surface hybridizes with the majority of the ketone groups upon RT deposition and activates the amine by partial deprotonation after annealing to 420 K. The hybridization presumably enables the molecule to remain on the surface during the thermally activated tilting of the ketones, which creates a suitable geometry to react with a diamine-terminated module. The putative mechanism is illustrated in Figure 6 by a schematic drawing.

We found that, in general, the cyclocondensation is favored over the single imine formation. Moreover, we observed that dimers are the preferred products, but in the presence of an excess of tetraketone molecules, ketone-terminated trimers are preferred. The elongation to longer oligomers seems instead to be unfavorable.

Importantly, we found marked differences between supporting the employed reactants on gold, silver, and copper. Among the three coinage metals, silver gives the best compromise between adsorption strength and relatively weak chemical interaction: both molecules can be confined in the vicinity of the surface under conditions that facilitate the condensation reaction. On the Au(111) surface, the anchoring appears to be too weak to promote the condensation reaction, such that the majority of the tetraketone molecules desorbed when the temper-

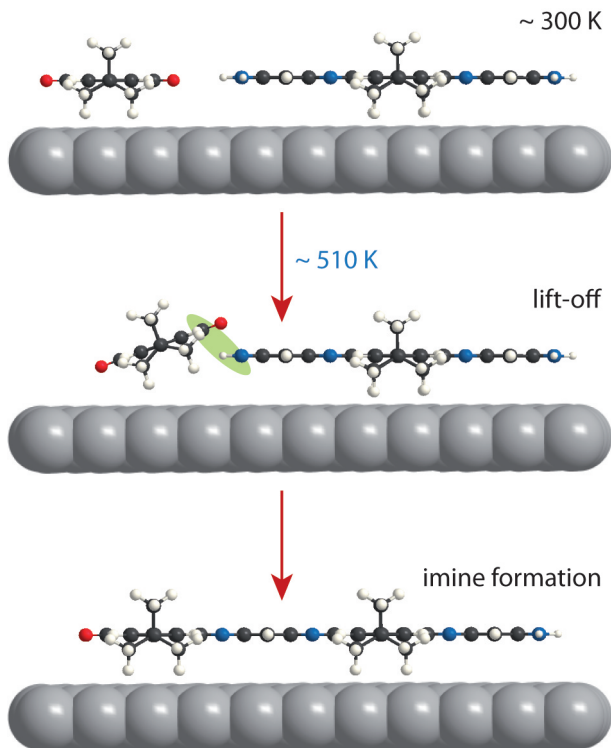


FIG. 6. Cartoon of the imine formation mechanism by reaction of tetraketone (left) and tetraamine (right) on the Ag(111) surface. From top to bottom: After RT deposition, ketone moieties are strongly hybridized with the metal surface. At  $\sim 510$  K, the ketone lift-off enables a suitable geometry (green highlight) for the formation of new imines.

ature was raised. On the contrary, the Cu(111) surface interacts too strongly with the molecules and resulted in decomposition rather than polymerization.

The combination of direct visualization of all reactants and reaction products with the spectroscopic characterization of the reactants has provided a unique mechanistic insight into the interfacial synthesis of PPA-based oligomers on solid surfaces, thereby offering a sound methodology for studying other on surface polymerization reactions. The findings reported are expected to provide valuable input in using imine formation for the desired extension of the conjugated nanostructures by rational design of appropriate building blocks, choice of platforms, and polymerization conditions.

## EXPERIMENTAL SECTION

**Synthesis.** The synthesis of tetraketone<sup>60</sup> and tetraamine<sup>16,61–63</sup> molecules was carried out following reported procedures.

**Sample Preparation.** Ag(111), Cu(111), and Au(111) single crystal surfaces were prepared by repeated cycles of Ar<sup>+</sup> sputtering and subsequent thermal annealing. The quality and cleanliness of the substrate sur-

face were assessed by STM or XPS. Tetraketone and tetraamine molecules were dosed by organic molecular beam epitaxy (by heating to  $\sim 470$  and  $\sim 650$  K, respectively) onto the substrates at room temperature under UHV conditions, from separate quartz crucibles. The deposition time was appropriately controlled to attain the desired molecular coverage.

**STM.** STM measurements were performed in a custom-made UHV system equipped with an Aarhus-type variable-temperature STM at a base pressure of  $2 \times 10^{-10}$  mbar. All STM images were recorded in constant-current mode using electrochemically etched tungsten tips and processed with the WsXM program.<sup>64</sup> The tunneling bias ( $U_s$ ) is applied to the sample.

**XPS.** XPS experiments of tetraamine on Ag(111) were carried out at the HE-SGM dipole magnet beamline at the BESSY II synchrotron facility in Berlin. The spectra were collected using a Scienta R3000 hemispherical electron energy analyzer mounted in the plane of the photon polarization,  $45^\circ$  from the incident photon beam. The N 1s and C 1s core levels were probed in normal emission with photon energies of 550 and 435 eV, respectively. Additional XPS measurements of tetraketone on Ag(111) and Au(111) were performed in a dedicated facility (SPECS GmbH) at the TUM-WSI laboratory in Garching. The experimental chamber operates at a base pressure of  $2 \times 10^{-10}$  and is equipped with a PHOIBOS 150 hemispherical analyzer, a XR50 X-ray source with ellipsoidal crystal FOCUS 500 monochromator (SPECS GmbH) delivering monochromatized Al K $\alpha$  radiation ( $h\nu = 1486.6$  eV), and all ancillary facilities for surface preparation and cleaning. The XPS experiments were conducted in normal emission geometry. The binding energy of the XP spectra was calibrated against the Ag 3d<sub>5/2</sub> or Au 4f<sub>7/2</sub> core levels at 368.3 and 84.0 eV, respectively. For the acquired XPS data, a Shirley background was subtracted from the raw data, and Voigt functions were used to fit the individual components.

## ACKNOWLEDGMENTS

This work was supported by the ERC Advanced Grant MolArt (No. 247299) and the Excellence Clusters Munich-Centre for Advanced Photonics (MAP) and Nanosystems Initiative Munich (NIM) funded by the German Research Foundation (DFG) via the German Excellence Initiative. L.J., Ö.S., and D.A.D. acknowledge funding from the China Scholarship Council (CSC), a Marie Curie International Incoming Fellowship (Project NANOULOP), and the Humboldt foundation, respectively. We thank the Helmholtz-Zentrum Berlin for the allocation of synchrotron radiation beamtime and financial support. Prof. Christof Wöll and Dr. Alexei Nevedov are gratefully acknowledged for support at the end station of the HE-SGM beamline, and Karl Eberle for assistance on the monochromatic XPS facility in Garching. A.M.A. acknowledges sup-

port from the Freiburg Institute for Advanced Studies (FRIAS), the Basque Science Foundation for Science (Ikerbasque), POLYMAT, the University of the Basque Country (SGIker), the Deutsche Forschungsgemeinschaft (AU 373/3-1 and MA 5215/4-1), Gobierno de España (Ministerio de Economía y Competitividad, MAT2012-35826), Gobierno Vasco (BERC program and PC2015-1-01(06-37)), Diputación Foral de Guipuzcoa (2015-CIEN-000054-01), and the European Union (ERA-Chemistry, Career Integration Grant No. 618247, and FEDER).

## ASSOCIATED CONTENT

The Supporting Information is available free of charge on the ACS Publications website at DOI: 10.1021/acsnano.5b06340. STM characterization data, reaction mechanism of imine formation in solution, total counts of surface species, and calculation of standard deviation

## REFERENCES

1. Kroto, H. W.; Heath, J. R.; O'Brien, S. C.; Curl, R. F.; Smalley, R. E. C60: Buckminsterfullerene. *Nature* **1985**, *318*, 162–163.
2. (2) Wang, H.; Maiyalagan, T.; Wang, X. Review on Recent Progress in Nitrogen-Doped Graphene: Synthesis, Characterization, and Its Potential Applications. *ACS Catal.* **2012**, *2*, 781–794.
3. (3) Zhao, L.; He, R.; Rim, K. T.; Schiros, T.; Kim, K. S.; Zhou, H.; Gutiérrez, C.; Chockalingam, S. P.; Arguello, C. J.; Pálová, L.; et al. Visualizing Individual Nitrogen Dopants in Monolayer Graphene. *Science* **2011**, *333*, 999–1003.
4. (4) Lv, R.; Li, Q.; Botello-Méndez, A. R.; Hayashi, T.; Wang, B.; Berkdemir, A.; Hao, Q.; Elías, A. L.; Cruz-Silva, R.; Gutiérrez, H. R.; et al. Nitrogen-Doped Graphene: Beyond Single Substitution and Enhanced Molecular Sensing. *Sci. Rep.* **2012**, *2*, 586.
5. Bronner, C.; Stremlau, S.; Gille, M.; Brauße, F.; Haase, A.; Hecht, S.; Tegeder, P. Aligning the Band Gap of Graphene Nanoribbons by Monomer Doping. *Angew. Chem., Int. Ed.* **2013**, *52*, 4422–4425.
6. Vo, T. H.; Shekhirev, M.; Kunkel, D. A.; Orange, F.; Guinel, M. J. F.; Enders, A.; Sinitskii, A. Bottom-Up Solution Synthesis of Narrow Nitrogen-Doped Graphene Nanoribbons. *Chem. Commun.* **2014**, *50*, 4172–4174.
7. (7) Cai, J.; Pignedoli, C. A.; Talirz, L.; Ruffieux, P.; Söde, H.; Liang, L.; Meunier, V.; Berger, R.; Li, R.; Feng, X.; et al. Graphene Nanoribbon Heterojunctions. *Nat. Nanotechnol.* **2014**, *9*, 896–900.
8. (8) Denk, R.; Hohage, M.; Zeppenfeld, P.; Cai, J.; Pignedoli, C. A.; Söde, H.; Fasel, R.; Feng, X.; Müllen, K.; Wang, S.; et al. Exciton-Dominated Optical Response of Ultra-Narrow Graphene Nanoribbons. *Nat. Commun.* **2014**, *5*, 4253.
9. Mateo-Alonso, A. Pyrene-Fused Pyrazaacenes: From Small Molecules to Nanoribbons. *Chem. Soc. Rev.* **2014**, *43*, 6311–6324.
10. Mateo-Alonso, A.; Ehli, C.; Chen, K. H.; Guldi, D. M.; Prato, M. Dispersion of Single-Walled Carbon Nanotubes with an Extended Diazapentacene Derivative. *J. Phys. Chem. A* **2007**, *111*, 12669–12673.
11. Mateo-Alonso, A.; Kulisic, N.; Valenti, G.; Marcaccio, M.; Paolucci, F.; Prato, M. Facile Synthesis of Highly Stable Tetraazaheptacene and Tetraazaoc-tacene Dyes. *Chem. - Asian J.* **2010**, *5*, 482–485.
12. Kulisic, N.; More, S.; Mateo-Alonso, A. A Tetraalkylated Pyrene Building Block for the Synthesis of Pyrene-Fused Azaacenes with Enhanced Solubility. *Chem. Commun.* **2011**, *47*, 514–516.
13. More, S.; Bhosale, R.; Choudhary, S.; Mateo-Alonso, A. Versatile 2,7-Substituted Pyrene Synthons for the Synthesis of Pyrene-Fused Azaacenes. *Org. Lett.* **2012**, *14*, 4170–4173.
14. More, S.; Bhosale, R.; Mateo-Alonso, A. Low-LUMO Pyrene-Fused Azaacenes. *Chem. - Eur. J.* **2014**, *20*, 10626–10631.
15. More, S.; Choudhary, S.; Higelin, A.; Krossing, I.; Melle-Franco, M.; Mateo-Alonso, A. Twisted Pyrene-Fused Azaacenes. *Chem. Commun.* **2014**, *50*, 1976–1979.
16. Gao, B. X.; Wang, M.; Cheng, Y. X.; Wang, L. X.; Jing, X. B.; Wang, F. S. Pyrazine-Containing Acene-Type Molecular Ribbons with up to 16 Rectilinearly Arranged Fused Aromatic Rings. *J. Am. Chem. Soc.* **2008**, *130*, 8297–8306.
17. Stille, J. K.; Mainen, E. L. Ladder Polyquinoxalines. *J. Polym. Sci., Part B: Polym. Lett.* **1966**, *4*, 665–667.
18. Stille, J. K.; Mainen, E. L. Thermally Stable Ladder Polyquinoxalines. *Macromolecules* **1968**, *1*, 36–42.
19. Imai, K.; Kurihara, M.; Mathias, L.; Wittmann, J.; Alston, W. B.; Stille, J. K. Synthesis and Properties of Thermally Stable Ladder Polymers Containing the 1,4-Pyrazine Ring Obtained from Polyheterocyclizations of Tetramines and Tetraketones in Poly(phosphoric acid) and m-Cresol. *Macromolecules* **1973**, *6*, 158–162.

20. Franc, G.; Gourdon, A. Covalent Networks through On-Surface Chemistry in Ultra-High Vacuum: State-of-the-Art and Recent Developments. *Phys. Chem. Chem. Phys.* **2011**, *13*, 14283–14292.
21. Mendez, J.; Lopez, M. F.; Martin-Gago, J. A. On-Surface Synthesis of Cyclic Organic Molecules. *Chem. Soc. Rev.* **2011**, *40*, 4578–4590.
22. Lackinger, M.; Heckl, W. M. A STM Perspective on Covalent Intermolecular Coupling Reactions on Surfaces. *J. Phys. D: Appl. Phys.* **2011**, *44*, 464011.
23. Björk, J.; Hanke, F. Towards Design Rules for Covalent Nanostructures on Metal Surfaces. *Chem. - Eur. J.* **2014**, *20*, 928–934.
24. Fan, Q.; Gottfried, J. M.; Zhu, J. Surface-Catalyzed C–C Covalent Coupling Strategies toward the Synthesis of Low-Dimensional Carbon-Based Nanostructures. *Acc. Chem. Res.* **2015**, *48*, 2484–2494.
25. Dong, L.; Liu, P. N.; Lin, N. Surface-Activated Coupling Reactions Confined on a Surface. *Acc. Chem. Res.* **2015**, *48*, 2765–2774.
26. Klappenberger, F.; Zhang, Y.-Q.; Björk, J.; Klyatskaya, S.; Ruben, M.; Barth, J. V. On-Surface Synthesis of Carbon-Based Scaffolds and Nanomaterials Using Terminal Alkynes. *Acc. Chem. Res.* **2015**, *48*, 2140–2150.
27. Bebensee, F.; Bombis, C.; Vadapoo, S. R.; Cramer, J. R.; Besenbacher, F.; Gothelf, K. V.; Linderoth, T. R. On-Surface Azide-Alkyne Cycloaddition on Cu(111): Does it “Click” in Ultrahigh Vacuum? *J. Am. Chem. Soc.* **2013**, *135*, 2136–2139.
28. Díaz Arado, O.; Mönig, H.; Wagner, H.; Franke, J.-H.; Langewisch, G.; Held, P. A.; Studer, A.; Fuchs, H. On-Surface Azide-Alkyne Cycloaddition on Au(111). *ACS Nano* **2013**, *7*, 8509–8515.
29. Zhang, Y.-Q.; Kepčija, N.; Kleinschrodt, M.; Diller, K.; Fischer, S.; Papageorgiou, A. C.; Allegretti, F.; Björk, J.; Klyatskaya, S.; Klappenberger, F.; et al. Homo-Coupling of Terminal Alkynes on a Noble Metal Surface. *Nat. Commun.* **2012**, *3*, 1286.
30. Wiengarten, A.; Seufert, K.; Auwärter, W.; Eciija, D.; Diller, K.; Allegretti, F.; Bischoff, F.; Fischer, S.; Duncan, D. A.; Papageorgiou, A. C.; et al. Surface-assisted Dehydrogenative Homocoupling of Porphine Molecules. *J. Am. Chem. Soc.* **2014**, *136*, 9346–9354.
31. Wiengarten, A.; Lloyd, J. A.; Seufert, K.; Reichert, J.; Auwärter, W.; Han, R.; Duncan, D. A.; Allegretti, F.; Fischer, S.; Oh, S. C.; et al. Surface-Assisted Cyclodehydrogenation; Break the Symmetry, Enhance the Selectivity. *Chem. - Eur. J.* **2015**, *21*, 12285–12290.
32. Zhong, D.; Franke, J.-H.; Podiyanachari, S. K.; Blömker, T.; Zhang, H.; Kehr, G.; Erker, G.; Fuchs, H.; Chi, L. Linear Alkane Polymerization on a Gold Surface. *Science* **2011**, *334*, 213–216.
33. Int Veld, M.; Iavicoli, P.; Haq, S.; Amabilino, D. B.; Raval, R. Unique Intermolecular Reaction of Simple Porphyrins at a Metal Surface Gives Covalent Nanostructures. *Chem. Commun.* **2008**, 1536–1538.
34. Riss, A.; Wickenburg, S.; Gorman, P.; Tan, L. Z.; Tsai, H.-Z.; de Oteyza, D. G.; Chen, Y.-C.; Bradley, A. J.; Ugeda, M. M.; Etkin, G.; et al. Local Electronic and Chemical Structure of Oligoacetylene Derivatives Formed Through Radical Cyclizations at a Surface. *Nano Lett.* **2014**, *14*, 2251–2255.
35. Gao, H.-Y.; Held, P. A.; Knor, M.; Mück-Lichtenfeld, C.; Neugebauer, J.; Studer, A.; Fuchs, H. Decarboxylative Polymerization of 2,6-Naphthalenedicarboxylic Acid at Surfaces. *J. Am. Chem. Soc.* **2014**, *136*, 9658–9663.
36. Hu, F.-Y.; Zhang, X.-M.; Wang, X.-C.; Wang, S.; Wang, H.-Q.; Duan, W.-B.; Zeng, Q.-D.; Wang, C. In Situ STM Investigation of Two-Dimensional Chiral Assemblies through Schiff-Base Condensation at a Liquid/Solid Interface. *ACS Appl. Mater. Interfaces* **2013**, *5*, 1583–1587.
37. Liu, X.-H.; Guan, C.-Z.; Ding, S.-Y.; Wang, W.; Yan, H.-J.; Wang, D.; Wan, L.-J. On-Surface Synthesis of Single-Layered Two-Dimensional Covalent Organic Frameworks via Solid-Vapor Interface Reactions. *J. Am. Chem. Soc.* **2013**, *135*, 10470–10474.
38. Liu, X.-H.; Mo, Y.-P.; Yue, J.-Y.; Zheng, Q.-N.; Yan, H.-J.; Wang, D.; Wan, L.-J. Isomeric Routes to Schiff-Base Single-layered Covalent Organic Frameworks. *Small* **2014**, *10*, 4934–4939.
39. Tanoue, R.; Higuchi, R.; Enoki, N.; Miyasato, Y.; Uemura, S.; Kimizuka, N.; Stieg, A. Z.; Gimzewski, J. K.; Kunitake, M. Thermodynamically Controlled Self-Assembly of Covalent Nanoarchitectures in Aqueous Solution. *ACS Nano* **2011**, *5*, 3923–3929.
40. Tanoue, R.; Higuchi, R.; Ikebe, K.; Uemura, S.; Kimizuka, N.; Stieg, A. Z.; Gimzewski, J. K.;

- Kunitake, M. In Situ STM Investigation of Aromatic Poly(azomethine) Arrays Constructed by “On-Site” Equilibrium Polymerization. *Langmuir* **2012**, *28*, 13844–13851.
41. Tanoue, R.; Higuchi, R.; Ikebe, K.; Uemura, S.; Kimizuka, N.; Stieg, A. Z.; Gimzewski, J. K.; Kunitake, M. Positional Selectivity of Reversible Azomethine Condensation Reactions at Solid/Liquid Interfaces Leading to Supramolecule Formation. *J. Electroanal. Chem.* **2014**, *716*, 145–149.
  42. Xu, L.; Zhou, X.; Tian, W. Q.; Gao, T.; Zhang, Y. F.; Lei, S.; Liu, Z. F. Surface-Confined Single-Layer Covalent Organic Framework on Single-Layer Graphene Grown on Copper Foil. *Angew. Chem., Int. Ed.* **2014**, *53*, 9564–9568.
  43. Xu, L.; Zhou, X.; Yu, Y.; Tian, W. Q.; Ma, J.; Lei, S. Surface- Confined Crystalline Two-Dimensional Covalent Organic Frameworks via on-Surface Schiff-Base Coupling. *ACS Nano* **2013**, *7*, 8066–8073.
  44. Ciesielski, A.; El Garah, M.; Haar, S.; Kovaříček, P.; Lehn, J.-M.; Samori, P. Dynamic Covalent Chemistry of Bisimines at the Solid/ Liquid Interface Monitored by Scanning Tunnelling Microscopy. *Nat. Chem.* **2014**, *6*, 1017–1023.
  45. Weigelt, S.; Busse, C.; Bombis, C.; Knudsen, M. M.; Gothelf, K. V.; Strunskus, T.; Wöll, C.; Dahlbom, M.; Hammer, B.; Lægsgaard, E.; et al. Covalent Interlinking of an Aldehyde and an Amine on a Au(111) Surface in Ultrahigh Vacuum. *Angew. Chem., Int. Ed.* **2007**, *46*, 9227–9230.
  46. Alvarado, S. F.; Rieß, W.; Jandke, M.; Strohriegel, P. STM Investigation of Vapor-Deposition Polymerization. *Org. Electron.* **2001**, *2*, 75–82.
  47. Weigelt, S.; Busse, C.; Bombis, C.; Knudsen, M. M.; Gothelf, K. V.; Lægsgaard, E.; Besenbacher, F.; Linderoth, T. R. Surface Synthesis of 2D Branched Polymer Nanostructures. *Angew. Chem., Int. Ed.* **2008**, *47*, 4406–4410.
  48. Klappenberger, F. Two-Dimensional Functional Molecular Nanoarchitectures – Complementary Investigations with Scanning Tunneling Microscopy and X-ray Spectroscopy. *Prog. Surf. Sci.* **2014**, *89*, 1–55.
  49. Fischer, S.; Papageorgiou, A. C.; Lloyd, J. A.; Oh, S. C.; Diller, K.; Allegretti, F.; Klappenberger, F.; Seitsonen, A. P.; Reichert, J.; Barth, J. V. Self-Assembly and Chemical Modifications of Bisphenol A on Cu(111): Interplay Between Ordering and Thermally Activated Stepwise Deprotonation. *ACS Nano* **2014**, *8*, 207–215.
  50. Fischer, S.; Papageorgiou, A. C.; Marschall, M.; Reichert, J.; Diller, K.; Klappenberger, F.; Allegretti, F.; Nefedov, A.; Wöll, C.; Barth, J. V. L-Cysteine on Ag(111): A Combined STM and X-ray Spectroscopy Study of Anchorage and Deprotonation. *J. Phys. Chem. C* **2012**, *116*, 20356–20362.
  51. Huang, S. X.; Fischer, D. A.; Gland, J. L. Aniline Adsorption, Hydrogenation, and Hydrogenolysis on the Ni(100) Surface. *J. Phys. Chem.* **1996**, *100*, 10223–10234.
  52. Furukawa, M.; Yamada, T.; Katano, S.; Kawai, M.; Ogasawara, H.; Nilsson, A. Geometrical Characterization of Adenine and Guanine on Cu(110) by NEXAFS, XPS, and DFT Calculation. *Surf. Sci.* **2007**, *601*, 5433–5440.
  53. Lin, Y.-P.; Ourdjini, O.; Giovanelli, L.; Clair, S.; Faury, T.; Ksari, Y.; Themlin, J.-M.; Porte, L.; Abel, M. Self-Assembled Melamine Monolayer on Cu(111). *J. Phys. Chem. C* **2013**, *117*, 9895–9902.
  54. Davies, P. R.; Edwards, D.; Richards, D. STM and XPS Studies of the Oxidation of Aniline at Cu(110) Surfaces. *J. Phys. Chem. B* **2004**, *108*, 18630–18639.
  55. Moulder, J. F. *Handbook of X-ray Photoelectron Spectroscopy: A Reference Book of Standard Spectra for Identification and Interpretation of XPS data*; Physical Electronics Division, Perkin-Elmer Corporation, 1992.
  56. Rancan, M.; Sedona, F.; Di Marino, M.; Arme-lao, L.; Sambì, M. Chromium Wheels Quasi-Hexagonal 2D Assembling by Direct UHV Sublimation. *Chem. Commun.* **2011**, *47*, 5744–5746.
  57. Li, K.; Amann, T.; List, M.; Walter, M.; Moseler, M.; Kailer, A.; Rühe, J. Ultralow Friction of Steel Surfaces Using a 1,3-Diketone Lubricant in the Thin Film Lubrication Regime. *Langmuir* **2015**, *31*, 11033–11039.
  58. Heimel, G.; Duhm, S.; Salzmann, I.; Gerlach, A.; Strozecka, A.; Niederhausen, J.; Bürker, C.; Hosokai, T.; Fernandez Torrente, I.; Schulze, G.; et al. Charged and Metallic Molecular Monolayers through Surface-Induced Aromatic Stabilization. *Nat. Chem.* **2013**, *5*, 187–194.
  59. Papageorgiou, A. C.; Fischer, S.; Reichert, J.; Diller, K.; Blobner, F.; Klappenberger, F.; Allegretti, F.; Seitsonen, A. P.; Barth, J. V. Chemical Transformations Drive Complex Self-Assembly of Uracil on Close-Packed Coinage Metal Surfaces. *ACS Nano* **2012**, *6*, 2477–2486.

60. Hu, J.; Zhang, D.; Harris, F. W. Ruthenium(II) Chloride Catalyzed Oxidation of Pyrene and 2,7-Disubstitued Pyrenes: An Efficient, One-Step Synthesis of Pyrene-4,5-diones and Pyrene- 4,5,9,10-tetraones. *J. Org. Chem.* **2005**, *70*, 707–708.
61. Arnold, F. E. Ladder Polymers Containing Heterocyclic units of Different Structure. *J. Polym. Sci., Part B: Polym. Lett.* **1969**, *7*, 749– 753.
62. Arnold, F. E. Ladder Polymers from Tetraaminodiquinoxalpyrene. *J. Polym. Sci., Part A-1: Polym. Chem.* **1970**, *8*, 2079–2089.
63. Hedberg, F. L.; Arnold, F. E.; Kovar, R. F. Polyphenylquinoxalines with High Glass Transition Temperatures via Highly Fused Aromatic Tetraamines. *J. Polym. Sci., Polym. Chem. Ed.* **1974**, *12*, 1925–1931.
64. Horcas, I.; Fernández, R.; Gómez-Rodríguez, J. M.; Colchero, J.; Gómez-Herrero, J.; Baro, A. M. WSXM: A Software for Scanning Probe Microscopy and a Tool for Nanotechnology. *Rev. Sci. Instrum.* **2007**, *78*, 013705.